Received: 12 January 2019 | Revised: 5 June 2019 | Accepted: 5 June 2019

DOI: 10.4218/etrij.2018-0492

ORIGINAL ARTICLE

ETRI Journal WILEY

Exploiting W. Ellison model for seawater communication at gigahertz frequencies based on world ocean atlas data

Muhammad Tahir[1] | **Iftikhar Ali**[1] | **Piao Yan**[1] | **Mohsin Raza Jafri**[2] | **Jiang Zexin**[1] | **Di Xiaoqiang**[1]

[1]School of Electronics and Information Engineering, Changchun University of Science and Technology, Changchun, China

[2]Department of Environmental Sciences, Informatics and Statistics, Università Ca' Foscari, Venezia, Italy

Correspondence
Piao Yan, School of Electronics and Information Engineering, Changchun University of Science and Technology, Changchun, China.
Email: piaoyan@cust.edu.cn

Funding information
This research work to exploite W.Ellison Model for Seawater permittivity at GHz frequency based on WOA (2013) data sponsored by Ministry of Science and Technology under Project no: 2015DFR10670, School of Electronics and Information Engineering, Changchun University of Science and Technology, P.R.China.

Electromagnetic (EM) waves used to send signals under seawater are normally restricted to low frequencies (f) because of sudden exponential increases of attenuation (α) at higher f. The mathematics of EM wave propagation in seawater demonstrate dependence on relative permeability (μ_r), relative permittivity (ε_r), conductivity (σ), and f of transmission. Estimation of ε_r and σ based on the W. Ellison interpolation model was performed for averaged real-time data of temperature (T) and salinity (S) from 1955 to 2012 for all oceans with 41 088 latitude/longitude points and 101 depth points up to 5500 m. Estimation of parameters such as real and imaginary parts of ε_r, ε_r', ε_r'', σ, loss tangent (tan δ), propagation velocity (V_p), phase constant (β), and α contributes to absorption loss (L_a) for seawater channels carried out by using normal distribution fit in the 3 GHz–40 GHz f range. We also estimated total path loss (L_{PL}) in seawater for given transmission power P_t and antenna (dipole) gain. MATLAB is the simulation tool used for analysis.

KEYWORDS

absorption loss (L_a), normal distribution fit, seawater, total path loss (L_{PL}), W. Ellison interpolation model

1 | INTRODUCTION

The oldest known application of electromagnetic (EM) waves in seawater is the magnetic compass used for navigation. EM sources such as dipoles, loop antennas, and so on, and sensors are useful tools found in many diverse areas of oceanographic study such as physical oceanography, seafloor geophysics, marine chemistry, and marine biology. Advanced development of EM wave applications within these scientific disciplines has also been applied to emerging seawater navigation engineering systems. Applications include oil and gas exploitation and recovery, commercial fishing, weather prediction, tsunami warning, and underwater wireless communication technology [1]. EM communication also has important applications in geophysical surveys and investigation of the seafloor. Acoustic waves with low propagation velocities (~1500 m/s) can travel long distances in seawater with minimum attenuation. However, EM waves in seawater provide higher data rates at short ranges, with reliable communication across the sea/air boundary. Maxwell's equations regarding the electric and magnetic field properties in a conducting medium (seawater) have helped develop mathematical descriptions of EM fields using dipole sources within seawater [2].

The strong covalent bond between hydrogen (H) and oxygen (O) atoms in seawater molecules cause no free electrons in the conduction band until they jump to a higher energy level upon application of a high-amplitude electric field, E. Fresh water, which has a lower σ value than seawater (~0.01 S/m), undergoes dielectric breakdown upon application of an electric field of a few megavolts per centimeter (MV/cm). This dielectric breakdown creates an electric arc. However, the salt in seawater dissociates into positive and negative ions, making seawater a good electric conductor at all E field levels. Seawater with an applied E can be treated as a conductor with σ ranging from ~2.5 S/m in cold deep waters to ~6 S/m in very warm waters [3]. The value of σ typically used in the literature for open ocean is ≈4 S/m. Seawater is also considered non-magnetic due to its permeability, μ (H/m), which is the same as that of free space ($\mu_0 = 4\Pi \times 10^{-7}$) H/m [4].

In the tropics, where there is an excess of primarily short waves from incoming solar radiation as compared to outgoing long-wave radiation, the surface waters are warmer (with a maxima of 25 °C to 30 °C) than those at adjacent latitudes. In contrast, surface waters at higher latitudes are cooler, with the freezing point of seawater around −2 °C. The waters in these latitudes are cooler because energy lost to the atmosphere and outer space by outgoing long-wave radiation exceeds incoming solar radiation. Figure 1 shows global ocean surface temperatures, reflecting tropical warming and polar cooling. However, the distribution of T with latitude varies zonally due to variations of general oceanographic circulation patterns with the seasons. Historically, the ocean's S value was determined by chemical titration of a sample collected in a bottle lowered on a wire from ship. In the 1970s, considerable research was conducted on both the definition and measurement of σ to state seawater S. Technological advancements helped in measuring S, which was averaged from 1955 to 2012. The results are depicted in Figure 2 [5].

Acoustic waves are a major source for seawater communications and for tracking and telemetry applications. There are no alternatives to acoustic waves in long-range R (meters) applications, in spite of drawbacks such as multipath fading, narrow bandwidth, and susceptibility to propagation characteristics from background media such as animal noises and noise near the surface of the ocean from the movement of ships. Underwater electromagnetic wave (EMW) communication in the 100-m range was studied for half a century before 1970 using low-frequency underwater modems. High-frequency (GHz) EMWs can propagate through seawater with low damping to compensate for the shortcomings of acoustic waves considering the digital technology revolution in last few decades [6]. Figure 3 shows underwater wireless communication (UWC) architecture in a seawater environment. Sensor nodes can be both mobile and static and can deliver information data

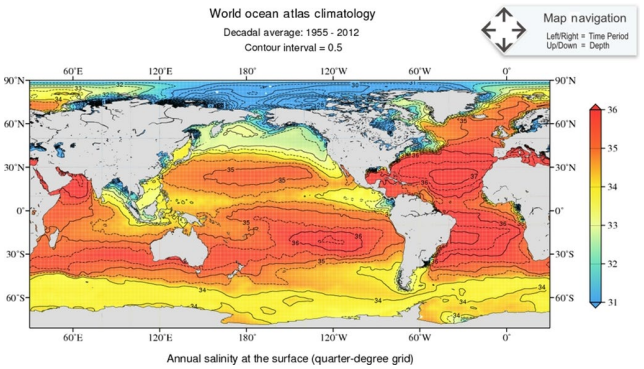

FIGURE 2 Mean seawater surface S (ppt) averaged from 1955 to 2012.Mishonov, Alexey National Center for Atmospheric Research Staff (Eds). Last modified 13 October 2016. "The Climate Data Guide: World Ocean Atlas 2013 (WOA13)." Retrieved from https://climatedataguide.ucar.edu/climate-data/world-ocean-atlas-2013-woa13

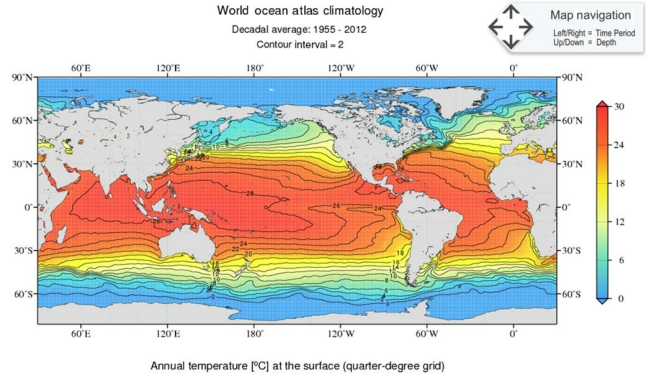

FIGURE 1 Mean seawater surface temperature T (°C) averaged from 1955 to 2012. Mishonov, Alexey National Center for Atmospheric Research Staff (Eds). Last modified 13 October 2016. "The Climate Data Guide: World Ocean Atlas 2013 (WOA13)." Retrieved from https://climatedataguide.ucar.edu/climate-data/world-ocean-atlas-2013-woa13

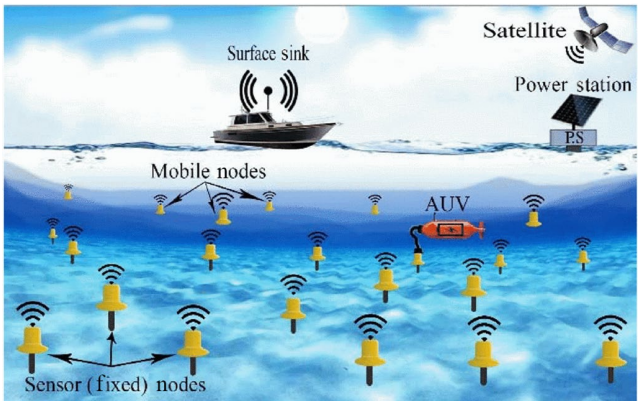

FIGURE 3 UWC network architecture. © 2018 IEEE. Reprinted with permission from [M. Mostafa et al., *A comparative study on underwater communications for enabling C/U plane splitting based hybrid UWSN*, in Proc. IEEE Wireless Commun. Netw. Conf. (Barcelona, Spain), Apr. 2018]

to mobile autonomous underwater vehicles (AUVs) that establish an offshore link with the surface sink (the ship) [7].

2 | LITERATURE REVIEW AND MOTIVATION

Acoustic waves can travel at 1500 m/s, much slower than the propagation speed (V_p) of EM waves in seawater, which is approximately 3×10^7 m/s. This causes channel latency and Doppler effects for traveling acoustic signals. Oceans act as a waveguide for acoustic signals as they provide boundaries by the upper surface and the sea floor. Consequently, reflections from these surfaces must be considered and shadow zones need to be addressed. The main advantage of acoustic communication is its ability to propagate over large distances, which makes it a frequently used and successful communication technique [8]. Optical signals are also a mode of communication in seawater; however, they are generally used only for short-range data transfer. Their use is being explored in shallow waters (~100 m) where acoustic communication seems to be less effective due to manmade noise near the surface of the ocean. Optical signals can provide higher bandwidths and higher data rates as compared to acoustic signals. The main limitations for optical signals include rapid attenuation (α) and the scattering effect of particles suspended in seawater [9].

Underwater wireless sensor networks (UWSNs) are combinations of sensors used to monitor physical or environmental phenomena such as humidity, temperature, sound, vibration, pressure, or motion. Data are cooperatively passed through this network of sensors to a main sink. UWSNs are becoming smaller and cheaper to use for EM signaling. Because of the high attenuation of EM signals in seawater, UWSNs rely on sonic transducers for wireless communication. The use of more nodes to overcome high path loss (L_{PL}) and attenuation in seawater contributes to the higher cost of EM signaling. EM waves reduce latency due to faster propagation and provide high data rates due to the high frequency of transmitted EM waves. Antennas for EM wave propagation in seawater must meet a number of requirements to overcome high path loss. For example, they must have high gain for both the transmitter and the receiver (G_T and G_R, respectively), that is, above 10 dB, and they must be small so that they can be fitted on a sensor surface. Most common antennas used for seawater communication using EM signals are bow-tie antennas, dipoles, loops, and so on [10].

Significant advantages of EM propagation across seawater include an efficient antenna system that can be easily transported in compact units and immunity to acoustic noise and low-visibility areas. Over the past decade, digital technology has rapidly improved, leading to high data-rate communication systems such as Bluetooth that make valuable use of high bandwidth and short-range technologies [11]. Major examples of these applications are communication between unmanned underwater vehicles (UUVs), submarines, or surface vessels, as well as diving communication and navigation. [12]

EM waves traveling in seawater in a positive z-direction are governed by Maxwell's equations. The electric (E) and magnetic (H) fields are described as follows in (1) and (2), respectively: [13]

$$E_x = E_0 e^{j\omega t - \gamma z} \tag{1}$$

and

$$H_y = H_0 e^{j\omega t - \gamma z}. \tag{2}$$

The propagation constant (γ) of a medium, which depends on frequency (f), conductivity (σ), permittivity (ε), and permeability (μ) is presented in (3) [13].

$$\gamma = j\omega\sqrt{\mu_0\mu_r\left(\varepsilon_0\varepsilon_r - j\sigma/\omega\right)} = \alpha + j\beta. \tag{3}$$

Here, α (Np/m) represents the attenuation factor and β (rad/m) represents the phase factor for traveling EM waves in seawater. For seawater, μ_r is 1, which leaves us with only two variables in the analysis of γ. Returning to (3), there are two solutions, depending on the transition frequency, $f_T = \omega_T/2\pi$. The first is a solution for the conduction band, where the ratio of the conductivity and transmitted frequency is greater than the permittivity of seawater ($\sigma/\omega > \varepsilon$), and the second is for the dielectric band, where the ratio of the conductivity and transmitted frequency is less than the permittivity of seawater ($\sigma/\omega < \varepsilon$) [14]. Debye's theory describes the relationship between the relative permittivity, ε_r, and the frequency, f, of EM waves in seawater. Debye makes the following assumptions [15]: (a) Water molecules are free and do not interact with each other; and (b) polarization contains induced and oriented components. The Debye model for ε_r is described as follows: [15]

$$\varepsilon_r = \varepsilon_r' - \varepsilon_r'' = \varepsilon_\infty + \left(\varepsilon_s - \varepsilon_\infty/1 + j\omega\tau\right) + j\sigma/\omega\varepsilon_0. \tag{4}$$

Here, ε_∞ equals ε at optical frequencies, ε_0 represents static ε, and τ is the relaxation time (s). ε_r' represents the real part of ε_r and ε_r'' represents the imaginary part of ε_r; σ is the ionic conductivity. The relaxation time, τ, taken by the dielectric to reach a state of equilibrium is defined by (5) [13].

$$\tau = \varepsilon/\sigma. \tag{5}$$

The conductivity, σ, of seawater is a function of T (°C) and S (ppt), denoted as $\sigma\,(T \cdot S)$ for a given range $-2\ °C \le T \le 30\ °C$

and 20 ppt $\leq S \leq$ 40 ppt, which leads to straightforward interpolation functions as represented in (6)–(10) [15].

$$\sigma(T,S) = c_1(T) + c_2(T)\,S. \tag{6}$$

The coefficients c_1 and c_2 are given in (7) and (8), respectively [15].

$$c_1(T) = 0.086 + 0.030T - 4.121\times10^{-4}T^2 \tag{7}$$

and

$$c_2(T) = 0.077 + 0.001T + 1.937\times10^{-5}T^2. \tag{8}$$

For f in the range of 3 GHz $\leq f \leq$ 40 GHz, T in range -2 °C $\leq T \leq$ 30 °C, and S (ppt) in the range 20 ppt $\leq S \leq$ 40 ppt. The ε_r value of seawater, denoted as $\varepsilon_r(f \cdot T \cdot S)$, is given with a precision of about 3% based on the W. Ellison model; it is described in terms of ε_r' and ε_r'' in (9) and (10), respectively [15].

$$\varepsilon_r'(f,T,S) = \varepsilon_\infty(T,S) + \left(\varepsilon_s(T,S) - \varepsilon_\infty(T,S)\right) \Big/ \left(1 + 4\Pi^2 f^2 \tau^2(T,S)\right) \tag{9}$$

and

$$\varepsilon_r''(f,T,S) = \left(\left(\varepsilon_s(T,S) - \varepsilon_\infty(T,S)\right) 2\Pi f \tau(T,S)\right) \Big/ \left(1 + 4\Pi^2 f^2 \tau^2(T,S)\right) + \sigma(T,S)/2\Pi\varepsilon_0 f. \tag{10}$$

Here, $\varepsilon_0 = 8.8419\times10^{-12}$ F/m, ε_s and τ for the given range are defined in (11) and (12), respectively [15].

$$\varepsilon_s(T,S) = a_1(T) + S a_2(T) \tag{11}$$

and

$$\tau(T,S) = b_1(T) + S b_2(T). \tag{12}$$

The estimated coefficients $a_i(t)$ and $b_i(t)$ for $i = 1, 2$ by least square regression analysis are described in (13)–(16) [15].

$$a_1(T) = 81.820 - 0.060T - 0.031T^2 + 0.003T^3 - 1.179*10^{-4}T^4 + 1.483*10^{-6}T^5, \tag{13}$$

$$a_2(T) = 0.125 + 0.009T - 9.55*10^{-4}T^2 + 9.88*10^{-5}T^3 - 3.061*10^{-6}T^4 + 4.713*10^{-8}T^5, \tag{14}$$

$$b_1(T) = 17.303 - 0.666T + 0.005T^2 + 0.001T^3 - 5.032*10^{-5}T^4 + 5.827*10^{-7}T^5, \tag{15}$$

$$b_2(T) = -0.006 + 2.357*10^{-4}T + 5.076*10^{-4}T^2 - 6.398*10^{-5}T^3 + 2.463*10^{-4}T^4 - 3.067*10^{-8}T^5. \tag{16}$$

The interpolation function for $\varepsilon_\infty(T,S)$ is given in (17) [15].

$$\varepsilon_\infty(T,S) = 6.458 - 0.042T - 0.006T^2 + 6.492*10^{-4}T^3 - 1.232*10^{-5}T^4 + 5.043*10^{-8}T^5. \tag{17}$$

The terms α and β depend on the dielectric properties of seawater given by Helmholtz model, formulated in (18) and (19), respectively, as [16]

$$\alpha = 2\pi/\lambda_0 \sqrt{1/2\varepsilon' \left(\sqrt{1 + (\varepsilon''/\varepsilon')^2} - 1\right)} \tag{18}$$

and

$$\beta = 2\pi/\lambda_0 \sqrt{1/2\varepsilon' \left(\sqrt{1 + (\varepsilon''/\varepsilon')^2} + 1\right)}. \tag{19}$$

Here, λ_0 represents the free-space wavelength (c/f).

The term $\tan(\delta)$ is an important factor that describes the characteristics of a material (lossy or dielectric) and v_p is the propagation velocity in seawater. [13]

$$\tan(\delta) = \sigma/\omega\varepsilon \tag{20}$$

and

$$v_p = \omega/\beta. \tag{21}$$

The penetration depth d_p for lossy material (seawater) can be estimated as [13]

$$d_p = 1/\alpha. \tag{22}$$

Finally, the overall path loss in seawater, L_{PL}, can be estimated as a combination of absorption loss L_a and free-space loss L_0, as depicted in (22) and (23), respectively. Here, P_T and P_R represent the transmitter and receiver power, respectively, G_T and G_R represent the transmitter and receiver antenna gains, respectively. The first part of equation represents the free-space loss, L_0, and the other part represents the absorption loss, L_a. The overall path loss, L_{PL}, can be depicted as the difference between the transmitter and receiver power $P_R - P_T$. Similarly, d represents the separation between the transmitter and receiver and the λ propagation wavelength of the signal transmitted [13].

$$P_R = P_T G_T G_R (\lambda/4\pi d)^2 \times e^{-2\alpha d} = P_{TG_TG_R \times L_0 \times L_a} \tag{23}$$

and

$$L_{PL}(\text{dB}) = P_T(\text{dBm}) + G_{T,R}(\text{dB}) - 20\log(4\pi d/\lambda) - 20\log\left(e^{\alpha d}\right). \tag{24}$$

The absorption of EM waves in the gigahertz range occurs due to the dielectric properties of seawater. This can help us examine a method for frequency control in applications such as submarine to satellite and radar communication. It also confirms possibilities of the absorption band and how a low σ value can absorb EM waves across a wide frequency band [17]. The terms ϵ_r and σ rapidly change in gigahertz frequency ranges, which motivated us to estimate accurate values for the given parameters across all latitude/longitude points for multiple depths of seawater. There are application areas that require perfect absorption of EM waves, such as military appliances, warships, and communication facilities, which should not be detected by radar in the gigahertz range. Radars generally determine the location of a target by absorbing EM waves and measuring their reflection from the surroundings. A new type of absorber suggested in research is seawater at a gigahertz frequency. These types of applications led us to estimate ϵ_r and σ, which contributes to the α value of the EM signal in seawater. The term tan δ determines the characteristics of seawater (Conductor, insulator, or dielectric) at multiple frequencies.

3 | SIMULATION RESULTS AND DISCUSSION

We analyzed the performance of the W. Ellison model based on real-time data averaged across multiple decades from 1955 to 2012 by using a normal distribution fit. We evaluated the performance of σ and ϵ_r in seawater depths from 5 m to 5500 m, along with L_{PL} versus an achievable distance in seawater. The simulation parameters are depicted in Table 1.

Figure 4 clearly indicates that we cannot assume constant $T = 20$ °C for oceans. The figure shows T on the y-axis and the number of occurrences with normal distribution fit (NDF) along the x-axis. We can see that T remains approximately constant between −2 °C and 2 °C up to a depth of 400 m. As we go deeper than 400 m, we can see that T starts to increase linearly to 30 °C. From a depth of 2500 m, T starts to decrease linearly up to approximately 3500 m. From there to a depth of 5500 m, it remains constant again in the range from −2 °C to 2 °C, with the greatest number of occurrences between 10 °C and 30 °C.

Figure 5 shows the S averaged data between 1955 and 2012 at different depth points (101) up to 5500 m. From the

TABLE 1 Simulation parameters

Oceans	Indian, Southern, Pacific, Atlantic, Arctic
Seawater depth (m)	5 to 5500
Seawater depth points	101 (distributed non-uniformly)
Latitude/Longitude	(0 to ±90)/ (0 to ±180)
Latitude/Longitude Points	41 088
Frequency range for analysis	3 GHz ≤ f ≤49 GHz
P_T for analysis	30 dBm
$G_{T,R}$ for analysis	10

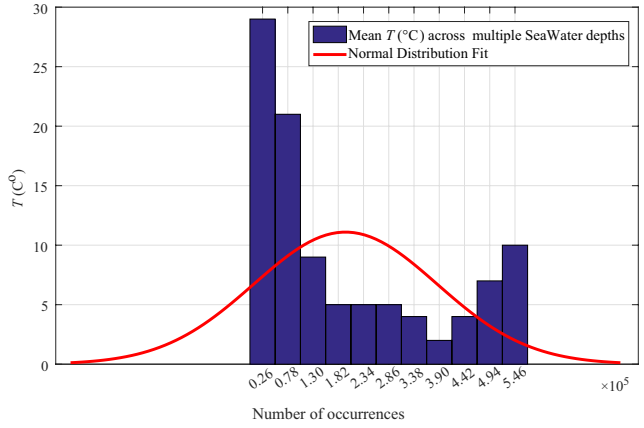

FIGURE 4 T (°C) for various seawater depths with NDF

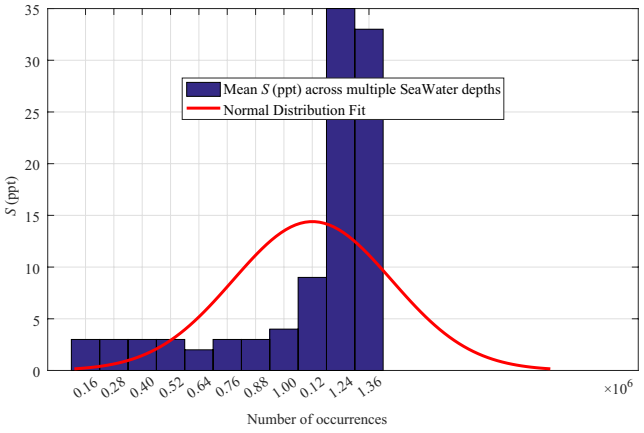

FIGURE 5 S values (ppt) for various seawater depths with NDF

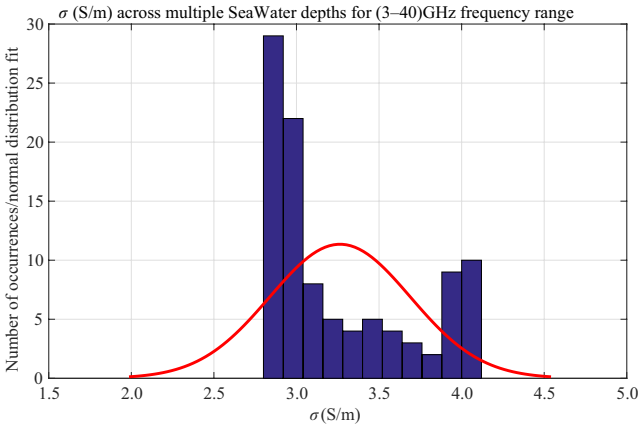

FIGURE 6 σ values (S/m) for various depths of seawater with NDF

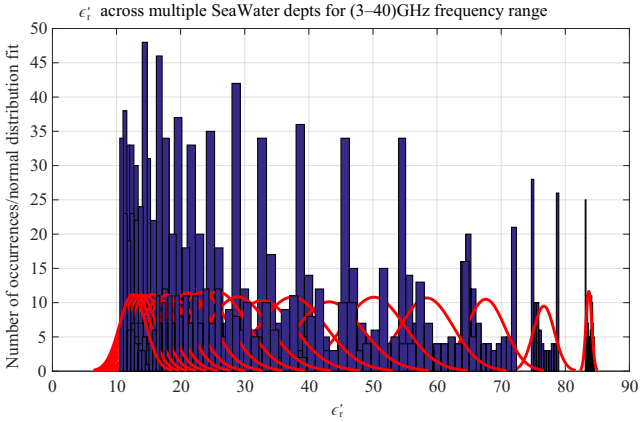

FIGURE 7 ε_r' values for various depths of seawater with NDF

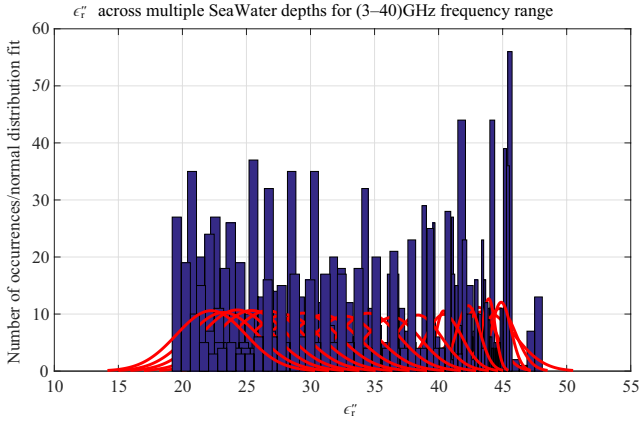

FIGURE 8 ε_r'' values for various seawater depths with NDF

seawater surface to a depth of 2000 m, the S value remained steady at around 35 ppt. From 2000 m up to 5500 m, S spreads in a non-uniform pattern between 5 ppt and 35 ppt. This is a clear deviation from standard assumption of S. It also defines characteristics at random seawater depths in nature.

Figure 6 shows σ values with NDF along multiple seawater depths estimated based on (6). It also shows variation of σ (S/m) with frequency with mean value of σ (S/m) between (2.8 to 4.2). ε_r' defines the energy dissipation of E (V/m) due to seawater molecule polarization which is normally assumed (≈81) at all frequencies and ocean depths. Figure 7 clearly indicates that ε_r' cannot be assumed constant across all seawater depths and frequency ranges (3 GHz to 40 GHz) estimated using the model given in (9). At 3 GHz, ε_r' is approximately 85, and as the seawater depth increases, it goes to 10. Similarly, we see at 40 GHz that the seawater surface ε_r' is approximately 18. As the depth of seawater increases, it reaches a minimum value of 10.

ε_r'' represents the loss in energy due to the conductivity of seawater and the vibration of seawater molecules when subjected to an electric field. In Figure 8, we can see that ε_r'' changes both with depth and frequency based on (10). At 3 GHz, ε_r'' is approximately 48 at the seawater surface. As we go deeper, it starts decreasing and reaches a minimum value of 3 at 5500 m. At 40 GHz, the value of ε_r'' varies from 25 to 2 in extreme depths. Figure 8 also depicts the low-frequency behavior of seawater, which is close to that of a conductor. As the frequency increases, seawater behaves like an insulator.

Table 2 shows values for the estimated parameters α, σ, V_p, $d_p \approx 1/\alpha$, $\tan\delta$, ε_r'', and ε_r' for a 5-m depth at multiple frequencies. It also includes the 3.1 GHz frequency for Wi-Fi communication in seawater. Figure 9 shows α values estimated based on the Helmholtz model mentioned for (18) using real-time data of all oceans (Indian, Pacific, Southern, Atlantic, and Arctic) averaged between 1955 and 2012. The value of α remains approximately constant up to 4000 m; beyond this up to 5500 m, it starts to decrease. For 3 GHz at the seawater surface, α is 20 dB/m, and as we go deeper, it is nearly 14. Similarly, for 40 GHz at the surface, α is 34 dB/m; at the extreme depth point, it is 27 dB/m. At low frequencies, the gap between α values is large as compared to higher frequencies.

The loss tangent ($\tan\delta$) parameter of a dielectric material quantifies its inherent dissipation of EM energy. It is an important factor for recognizing the type of material, whether it is a lossy dielectric, a lossless dielectric, or good conductor. In Figure 10, we estimated $\tan\delta$ based on (20) at multiple frequencies. Across seawater depths up to 500 m, $\tan\delta$ increases linearly. As we go deeper, $\tan\delta$ remains approximately constant. The seawater surface range of $\tan\delta$ is 0.46–1.85, and at extreme seawater depths it is 0.45 to 1.82. At 3 GHz, the initial value

TABLE 2 Estimated parameters for 5-m depth at multiple frequencies

Parameters	3 GHz	3.1 GHz	10 GHz	20 GHz	30 GHz	40 GHz
α(Np/m)	1.056*e*+02	1.64*e*+02	5.572*e*+02	1.258*e*+03	1.839*e*+03	2.2959*e*+03
σ(S/m)	4.050	4.050	4.050	4.050	4.050	4.050
V_p(m/s)	3.155*e*+07	3.250*e*+07	3.707*e*+07	4.557*e*+07	5.373*e*+07	6.094*e*+07
$d_p \approx 1/\alpha$(m)	0.0095	0.0083	0.0018	7.949*e*−04	5.437*e*−04	4.355*e*−04
tanδ	0.571	0.582	0.737	1.153	1.447	1.615
e_r''	47.967	47.032	43.057	39.549	32.692	26.983
e_r'	83.965	81.035	58.349	34.273	22.582	22.582

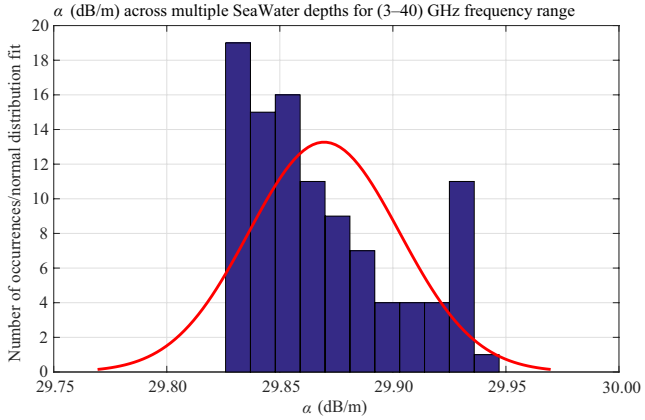

FIGURE 9 α values (dB/m) for various seawater depths with NDF

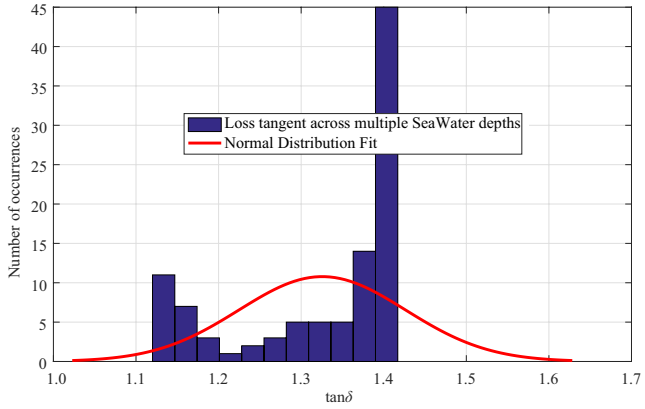

FIGURE 10 $\tan\delta$ values for various seawater depths with NDF

is 1.6, more like a conductor, but at 500 m, it goes to 1.82 and behaves more like an insulator. Similarly, for 40 GHz, the value starts from 0.46 and goes up to 0.45 at all seawater depths.

Table 3 shows the estimated values for the parameters α, σ, V_p, $d_p \approx 1/\alpha$, $\tan\delta$, ε_r'', and ε_r' for the 100-m depth at multiple frequencies. It also includes the 3.1 GHz frequency for Wi-Fi communication in seawater. β, the imaginary part of γ, contributes in estimating seawater and v_p. β also plays an important role in determining the phase change when EM waves cross the sea/air interface, estimated using the model depicted in (19). Figure 11

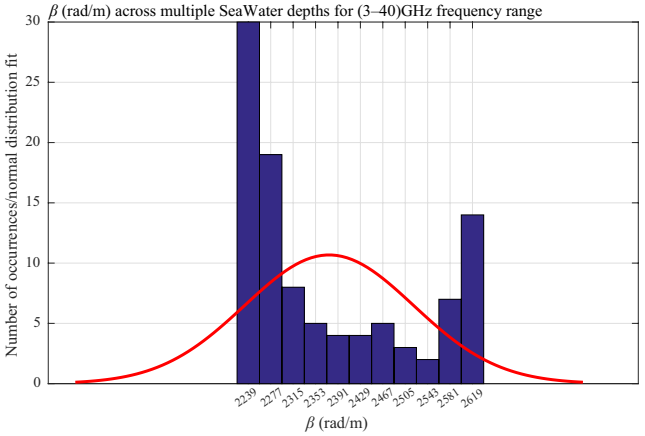

FIGURE 11 β values (rad/m) for various seawater depths with NDF

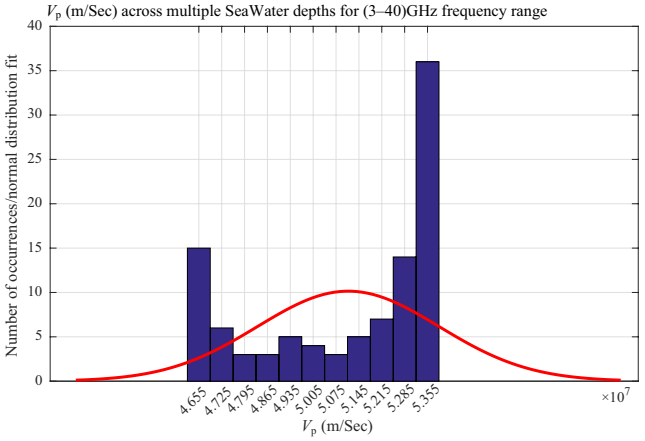

FIGURE 12 V_p values (m/s) for various depths of seawater with NDF

shows β values across the frequency range. At 3 GHz, β reaches a maximum value of 4000 rad/m at the seawater surface and starts decreasing, similar to α, reaching a minimum value of 1000 rad/m at extreme depths. At 40 GHz near the surface, β is approximately 500 rad/m, but at 5500 m, it is 100 rad/m.

The V_p values of EM waves in air (free space) are assumed to be approximately constant, 3×10^8 m/s. For seawater, the value mostly assumed in the literature is 3×10^7 m/s for each

TABLE 3 Estimated parameters for 100-m depth at multiple frequencies

Parameters	3 GHz	3.1 GHz	10 GHz	20 GHz	30 GHz	40 GHz
α(Np/m)	1.017*e*+02	1.627*e*+02	5.633*e*+02	1.258*e*+03	1.816*e*+03	2.247*e*+03
σ(S/m)	3.831	3.831	3.831	3.831	3.831	3.831
V_p(m/s)	3.206*e*+07	3.283*e*+07	3.798*e*+07	4.727*e*+07	5.606*e*+07	6.373*e*+07
$d_p \approx 1/\alpha$(m)	0.0098	0.0076	0.0018	7.949*e*−04	5.506*e*−004	4.450*e*−04
tanδ	0.556	0.573	0.770	1.220	1.526	1.690
e_r''	45.433	45.001	42.489	38.118	30.934	25.263
e_r'	81.578	80.037	55.117	31.223	20.260	14.945

TABLE 4 Estimated parameters for 500-m depth at multiple frequencies

Parameters	3 GHz	3.1 GHz	10 GHz	20 GHz	30 GHz	40 GHz
α (Np/m)	92.004	92.863	5.823e + 02	1.247e + 03	1.731e + 03	2.089e + 03
σ (S/m)	3.052	3.052	3.052	3.052	3.052	3.052
V_p (m/s)	3.329e + 07	3.699e + 07	4.044e + 07	5.222e + 07	6.278e + 07	7.155e + 07
$d_p \approx 1/\alpha$ (m)	0.0109	0.0100	0.0017	8.019e − 04	5.777e − 04	4.787e − 04
tanδ	0.518	0.563	0.872	1.420	1.730	1.843
ϵ_r''	39.588	39.953	41.253	34.225	26.342	20.918
ϵ_r'	76.336	75.001	47.256	24.0988	15.221	11.346

depth and frequency based on (21). We estimated $v_p$based on averaged real-time data for multiple decades at multiple depths in the world's oceans. In Figure 12, we can clearly see that at the seawater surface, v_p remains approximately constant up to 4000 m (0.25–0.65 $\times$ 10^7m/s). Beyond this depth, it starts increasing again exponentially up to 5500 m, achieving a maximum limit of 2.5 $\times$ 10^7. The range for V_p for extreme depths lies between 1.25 to 2.25 $\times$ 10^7 which is clearly different from the value that is normally assumed in the literature. Table 4 shows the values for the estimated parameters α, σ, V_p, $d_p \approx 1/\alpha$, tan δ, ϵ_r'', and ϵ_r' 500-m depth at multiple frequencies, including 3.1 GHz for Wi-Fi communication in seawater.

Figure 13 depicts the achievable distance in seawater considering the overall loss, L_a, L_0 for a given range of frequencies from 3 GHz to 40 GHz. The value of L_{PL} increases suddenly initially, but after a certain minimum distance, the overall loss remains approximately constant. For the analysis, we used a frequency range of 3 GHz to 40 GHz at P_T = 30 dBm and a transmitter and receiver antenna gain of $G_{T,R}$ = 10. The Rayleigh distance for the dipole antenna was approximately 5 m. The maximum achievable distance was 150 m, with maximum decay in transmission power. But for short-range communication within a few meters, gigahertz frequencies are a suitable choice in seawater. This can provide higher transmission data rates with minimum propagation delay.

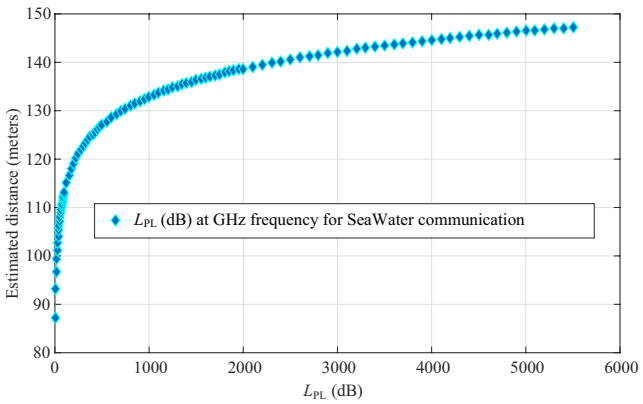

FIGURE 13 L_{PL} values for seawater communication at gigahertz frequencies

4 | CONCLUSION AND FUTURE WORK

This paper presents detailed analysis of the W. Ellison model parameters for seawater, ε_r and σ, based on real-time data for all oceans. We used specifically averaged annual data from 1955 to 2012 from the National Centre For Environmental Information (NCEI). An interpolation model for σ was analyzed for 3 GHz to 40 GHz at multiple depths. The analysis showed that the σ value varied from 4 to 0.01 on average for multiple frequencies. The ϵ_r' values at the seawater surface for multiple frequencies varied from 15 to 85, and at a seawater bottom depth of 5500 m, it ranged from 0.5 to 9.5 rather than remaining at a fixed value of 81. Similarly, the ϵ_r'' values for the seawater surface were between 25 and 45, and at maximum seawater depth, it was approximately 2–4. We also analyzed the channel performance for seawater based on the estimated total path loss L_{PL} versus achievable distance. From the results, it was clear that we can use gigahertz frequencies for seawater communication within a few meters; beyond that, the achievable distance is higher but with much higher L_{PL}. In the future we want to look at this problem in the context of e-navigation, bringing existing and new technologies together to improve safety of navigation, commercial efficiency, and security. Challenge for industries working through the International Maritime Organization (IMO) will be to produce a unified strategy for integration and to develop systems to meet the requirements through Smode. The concept of Smode is the default setting to bring all inputs such as radar, charts, and positioning for e-navigation to one platform. This all needs to be achieved through acceptable cost and benefits. E-navigation will be used for monitoring all kinds of activities in the world's oceans.

ORCID
Piao Yan https://orcid.org/0000-0002-4668-1193

REFERENCES

1. M. R. Dhanak and N. I. Xiros, Springer handbook of ocean engineering, Springer, Cham, Switzerland, 2016.
2. X. Che et al., *Re-evaluation of rf electromagnetic communication in under-water sensor networks*, IEEE Commun. Mag. **48** (2010), no. 12, 143–151.
3. R. Somaraju and J. Trumpf, *Frequency, temperature and salinity variation of the permittivity of seawater*, IEEE Trans. Antennas Propag. **54** (2006), no. 11, 3441–3448.
4. J. H. Jiang and D. L. Wu, *Ice and water permittivities for millimeter and sub-millimeter remote sensing applications*, Atmos. Sci. Lett. **5** (2004), no. 7, 146–151.
5. T. P. Boyer et al., World ocean database 2013., (2013).
6. H. Yoshida et al., *Measurements of underwater electromagnetic wave propagation*, in Proc. IEEE Underwater Technol. (Chennai, India), Feb. 2015, pp. 1–5.
7. M. Mostafa, H. Esmaiel, and E. M. Mohamed, *A comparative study on underwater communications for enabling C/U plane splitting based hybrid UWSNs*, in Proc. IEEE Wireless Commun. Netw. Conf. (Barcelona, Spain), Apr. 2018, pp. 1–6.
8. Y. K. Zahedi et al., *Feasibility of electromagnetic communication in underwater wireless sensor networks*, in Proc. Int. Conf. Inf. Eng. Inf. Sci. (Kuala Lumpur, Malaysia), Nov. 2011, pp. 614–623.
9. W. Chunbo and B. Liu, *Seawater electromagnetic propagation between two folded-dipoles at ism-band*, in Proc. Asia-Pacific Conf. Antennas Propag. (Xi'an, China), Oct. 2017, pp. 1–3.
10. A. Elrashidi et al., *Underwater wireless sensor network communication using electromagnetic waves at resonance frequency 2.4 GHz*, in Proc. Commun. Netw. Simulation Symp., Soc. Comput. Simulation Int. (Orlando, FL, USA), Mar., 2012, p. 13:1–7.
11. E. O'Shaughnessy, *Characterising the relative permittivity and conductivity of seawater for electromagnetic communications in the radio band-summary report 2012*, UNSW Canberra ADFA J. Undergraduate Eng. Res. **5** (2012), no. 1, 1–12.
12. M. A. Akkaş and R. Sokullu, *Channel modeling and analysis for wireless underground sensor networks in water medium using electromagnetic waves in the 300–700 mhz range*, Wireless. Pers. Commun. **84** (2015), no. 2, 1449–1468.
13. C. A. Balanis, *Advanced engineering electromagnetics*, John Wiley & Sons, Hoboken, NJ, 1999.
14. A. I. Al-Shamma'a, A. Shaw, and S. Saman, *Propagation of electromagnetic waves at mhz frequencies through seawater*, IEEE Trans. Antennas Propag. **52** (2004), no. 11, 2843–2849.
15. W Ellison et al., *New permittivity measurements of seawater*, Radio Sci. **33** (1998), no. 3, 639–648.
16. A. R. Von Hippel, *Dielectrics and waves*, New York, Wiley; London, Chapman & Hall, (1954).
17. M. Tahir, P. Yan, and L. Shuo, *Channel characterization of EM waves propagation at MHz frequency through seawater*, Int. J. Commun. Syst. **31** (2018), no. 3, e3462.

AUTHOR BIOGRAPHIES

Muhammad Tahir received his BS degree in Telecommunication Engineering and MS degree in Electrical Engineering from GC University Faisalbad and COMSATS University Islamabad in 2008 and 2013, respectively. He received his PhD in Information and Communication Engineering from School of Electronics and Information Engineering, Changchun University of Science and Technology, Changchun, China, in June 2019. His major research interests include RF/MW propagation, underwater wireless communication using EM waves, and energy optimization in WSNs.

Iftikhar Ali completed his MS on June 2019 in Computer Applied Technology from School of Computer Science and Technology, Changchun University of Science and Technology, Changchun, China. His major research interest includes underwater wireless communication and UWSNs.

Piao Yan received her PhD in Digital Signal Processing from Chinese Academy of Sciences, Changchun Institute of Optics and Fine Mechanics, China, in 2000. She is professor at School of Electronics and Information Engineering, Changchun University of Science and Technology, Changchun, China. Her major research interests include digital signal processing, wireless communication, image processing, and three-dimensional imaging technology.

Mohsin Raza Jafri completed his PhD in March 2019 majoring Computer Science from School of Environmental Sciences, Informatics and Statistics, Università Ca' Foscari Venezia, Italy. His major research interest includes wireless communication, WSNs, and UWSNs.

Jiang Zexin completed his MS on June 2019 in Information and Communication Engineering from School of Electronics and Information Engineering, Changchun University of Science and Technology, Changchun, China. His major research interests are Underwater image processing, Information processing and Underwater Wireless Communication.

Di Xiaoqiang is associate professor and vice dean of Information and Communication Center at School of Computer Science and Technology, Changchun University of Science and Technology, Changchun, China. His major research interests include wireless networks, software defined networks, network engineering, and satellite networks.